

Kinematic Limit Analysis of Periodic Heterogeneous Media¹

V. Carvelli², G. Maier², A. Taliercio²

Abstract: Homogenization of periodic fiber-reinforced ductile composite materials is performed as for the material strength, i.e. the carrying capacity with respect to macroscopic (average) stresses. Rigid-plastic limit analysis is formulated by the kinematic theorem applied to the representative volume with periodicity boundary conditions and von Mises yield criterion. The iterative procedure adopted for the numerical solution of the minimization problem is comparatively discussed on the basis of applications to various ductile heterogeneous media.

keyword: limit analysis, composites, periodic materials.

1 Introduction

At the present time heterogeneous materials are employed in several technological fields. When ductile constituents are adopted (such as in metal-matrix composites), the behaviour of these materials beyond the elastic range up to failure has to be investigated. Especially in the presence of periodic texture at the microscale, a mechanical and mathematical context in which heterogeneous media have been studied to structural engineering purposes is homogenization theory (see e.g. [Aboudi (1991)], [Nemat-Nasser and Hori (1993)], [Suquet (1985)], [Teply and Dvorak (1988)]). In this framework both step-by-step analyses (see e.g. [Michel and Suquet (1993)]) and “direct” methods (see e.g. [de Buhan and Maghous (1991)], [Francescato and Pastor (1997)], [Taliercio (1992)]) have been developed in order to numerically predict inelastic behaviour and in particular strength (or carrying capacity) of the homogenized material at the macroscale.

Evolutionary (“marching”) analyses generally provide a large amount of information but usually they turn out to be expensive and the provided information to be redundant. Nonevolutionary methods (otherwise called “direct” or “simplified”) may be convenient for limit state analyses of heterogeneous media, particularly when the design process requires repetitive parametric studies.

In this paper the kinematic approach of limit analysis will be formulated on the “representative volume” in the framework of the homogenization theory for ductile periodic media. An iterative algorithm, first proposed in [Huh and Yang (1991)], will be employed and comparatively discussed for the solution of

the mathematical programming problems which arise from finite element discretizations. Some aspects of the present study have been concisely outlined in [Carvelli, Maier and Taliercio (1998)].

2 Preliminaries on periodic heterogeneity

The underlying concept of homogenization theory is to replace a given heterogeneous medium by an “equivalent” homogeneous one with “same behaviour” at the macroscopic level. Homogenization techniques derive the mechanical properties of the homogenized medium in terms of the local geometrical and material (constitutive) properties of the constituents (or “phases”) at the microscale.

In order to generate macroscopic (homogenized) constitutive models for composite materials a ‘*statistical specimen*’ or ‘*representative volume*’ (*RV*) can be defined in different ways, consistently with the adopted homogenization technique (see e.g. [Hashin (1983)]). In heterogeneous media with a periodic structure, the *RV* is defined as the space region or “cell” with minimum volume among those which contain all information needed to completely describe geometric and physical properties at the microstructural level.

Let V be the volume occupied by the *RV* and Γ its boundary, in the Cartesian reference frame ($O x_1 x_2 x_3$). Any *RV* in the real medium is associated with a “macroscopic point” in the fictitious homogenized medium. In a *RV* two different kinds of variables can be considered: the macroscopic variables, concerning the homogenized medium (the material properties of which are sought), and the microscopic variables, which vary over the *RV*. Deformations will be assumed herein as “infinitesimal” (linear kinematics). The following symbols are adopted for the macroscopic (or “global”) stress and strain rate tensors, and for the microscopic (or “local”) stress and strain rate tensors, respectively: $\underline{\underline{\Sigma}}$, $\underline{\underline{\dot{E}}}$; $\underline{\underline{\sigma}}(\underline{x})$, $\underline{\underline{\dot{\epsilon}}}(\underline{x})$; tensors of second and of first order are represented by doubly or singly underlined symbols.

The macroscopic tensors are the averages of the microscopic ones over the *RV* [Suquet (1985)], namely:

$$\underline{\underline{\Sigma}} \equiv \frac{1}{V} \int_V \underline{\underline{\sigma}} dV \quad (1)$$

$$\underline{\underline{\dot{E}}} \equiv \frac{1}{V} \int_V \underline{\underline{\dot{\epsilon}}} dV = \frac{1}{2V} \int_{\Gamma} \text{sym}(\underline{\dot{u}} \otimes \underline{n}) d\Gamma \quad (2)$$

where $\underline{\dot{u}}(\underline{x})$ is the microscopic velocity field and \underline{n} is the out-

¹ Dedicated to Professor Leo Finzi on the occasion of his 75th anniversary.

² Department of Structural Engineering, Technical University (Politecnico) of Milan, Piazza Leonardo Da Vinci 32, 20133 Milan, Italy.

ward unit normal to Γ . Although discontinuous velocity fields are pertinent and useful in limit analysis and homogenization theory, only differentiable velocity fields will be considered herein.

If the heterogeneous body is subjected to boundary conditions that would produce uniform fields of strain $\underline{\underline{E}}$ rate and stress $\underline{\underline{\Sigma}}$ in the companion homogeneous body, then the microscopic strain rate $\underline{\underline{\dot{e}}}$ and $\underline{\underline{\sigma}}$ stress fields conform to the periodicity of the microscopic texture at a sufficiently large distance (large with respect to a typical RV length) from the boundary of the body. This means that one can write:

$$\underline{\underline{\dot{e}}}(\underline{x}) = \underline{\underline{E}} + \tilde{\underline{\underline{\dot{e}}}}(\underline{x}) \quad (3)$$

$$\underline{\underline{\sigma}}(\underline{x}) = \underline{\underline{\Sigma}} + \tilde{\underline{\underline{\sigma}}}(\underline{x}) \quad (4)$$

$$\underline{\underline{u}} = \underline{\underline{E}} \cdot \underline{x} + \tilde{\underline{\underline{u}}} \quad (5)$$

where $\underline{\underline{u}}$ is the velocity vector and a tilde marks addends which fluctuate with the periodicity of the microstructure. The “period” of the material texture is represented by any translation vector \underline{d} leading the RV to overlap on a neighbouring (identical) cell. Two points, say \underline{x}^A and \underline{x}^B , are called “homologous” if $\underline{x}^B = \underline{x}^A + \underline{d}$. It can be noticed from Eq. 1-4 that:

$$\frac{1}{V} \int_V \tilde{\underline{\underline{\dot{e}}}} dV = 0, \quad \frac{1}{V} \int_V \tilde{\underline{\underline{\sigma}}} dV = 0 \quad (6)$$

Eq. 4 implies that in two homologous points on the RV boundary Γ (where the outward normals are opposite to each other) the traction vector $\underline{t} = \underline{\underline{\sigma}} \cdot \underline{n}$ takes opposite values.

As a conclusion of what proceeds, the “periodicity conditions” read:

$$\underline{t} = \underline{\underline{\sigma}} \cdot \underline{n} \quad \text{anti-periodic} \quad (7)$$

$$\tilde{\underline{\underline{u}}} = \underline{\underline{u}} - \underline{\underline{E}} \cdot \underline{x} \quad \text{periodic} \quad (8)$$

Let us consider: a stress field $\underline{\underline{\sigma}}$ and a velocity field $\underline{\underline{u}}$ satisfying Eq. 7 and Eq. 8, respectively; a strain rate field $\underline{\underline{\dot{e}}}$ generated by $\underline{\underline{u}}$ through the (linear) compatibility operator and, hence, composed of two addends according to Eq. 3. These microscopic variables can be related to their macroscopic counterparts by Hill’s “macrohomogeneity equality” (see e.g. [Nemat-Nasser and Hori (1993)]):

$$\frac{1}{V} \int_V \underline{\underline{\sigma}} : \underline{\underline{\dot{e}}} dV = \underline{\underline{\Sigma}} : \underline{\underline{E}} \quad (9)$$

This equation, which plays an important role in homogenization theory, can be interpreted as a formulation of the virtual work principle applied to the RV .

3 Kinematic limit analysis with periodicity conditions

As a result of homogenization, limit loads of a heterogeneous structure can be obtained by analyzing an equivalent homogeneous structure subjected to the same loading conditions.

Limit loads are understood here as assigned external actions amplified by a critical value s (“safety factor”) of a common multiplier μ , such that $\mu > s$ cannot be sustained and for $\mu = s$ plastic collapse occurs. Under the assumption of periodic heterogeneity distribution, it can be proven (see e.g. [Bouchitte and Suquet (1991)] and [Suquet (1983)] that the “safety factor” of the fictitiously homogeneous structure tends to the one of the actual heterogeneous structure when the heterogeneity size becomes negligible compared to a typical structural length, provided that boundary conditions are fulfilled in a weak sense [Bouchitte and Suquet (1991)].

In order to perform overall limit analyses on the homogenized structure, the material macroscopic strength domain, denoted henceforth by S^{hom} , must be determined in the space of the macroscopic (average) stresses $\underline{\underline{\Sigma}}$. This is the present main objective. In classical plasticity under the “small deformation” hypothesis, it was established long ago that if Drucker’s postulate of material stability holds (with its associativity and convexity consequences) for the behaviours of the constituents, it holds for the overall behaviour as well [Maier and Drucker (1973)]. By the same path of reasoning, in the homogenization context, if the material constituents obey an associated flow rule (i.e. are “standard” in the sense of the plasticity theory) and if their yield domains $\phi(\underline{\underline{\sigma}}, \underline{x})$ are convex at any point of the RV , it can be proven that the domain S^{hom} of admissible average stresses $\underline{\underline{\Sigma}}$, is convex and the homogenized medium obeys the normality rule, see e.g. [Suquet (1985)]. Both these essential features are assumed herein and are supplemented by the hypothesis of perfect plasticity (no hardening). If the components were not “standard”, S^{hom} should be considered as the domain of the “potentially safe” macroscopic stresses for the homogeneous equivalent structure [Talierecio and Sagramoso (1995)].

In the presence of texture periodicity, rigid-perfectly plastic constituents stable in Drucker’s sense and perfect cohesion at the interfaces, the static and kinematic theorems of classical limit analysis (see e.g. [Cohn and Maier (1979)], [Lubliner (1990)]) can be applied to the RV alone. They provide the conceptual basis to homogenization procedures apt to compute the safety factor for a given “loading condition” $\underline{\underline{\Sigma}}^o$, and the macroscopic strength domain S^{hom} for all $\underline{\underline{\Sigma}}^o$. Specifically, by a kinematic approach, the definition of S^{hom} arises from the energy equation (Eq. 9) and from the kinematic theorem of limit analysis, namely: S^{hom} is the set of the macroscopic stresses $\underline{\underline{\Sigma}}$ whose “external” work rate $\underline{\underline{\Sigma}} : \underline{\underline{E}}$ (per unit volume) is bounded from above by the average microscopic (local) plastic dissipation D over the RV for any compatible strain rate field derived from a displacement rate field which complies with the decomposition Eq. 5 and with the periodicity condition (Eq. 8). Namely, in symbols:

$$S^{hom} \equiv \left\{ \underline{\underline{\Sigma}} \text{ such that: } \underline{\underline{\Sigma}} : \underline{\underline{E}} \leq \frac{1}{V} \int_V D \left[\underline{\underline{\dot{e}}}(\underline{\underline{u}} + \underline{\underline{E}} \cdot \underline{x}) \right] dV \right.$$

$$\forall \underline{\dot{\mathbf{E}}}, \underline{\dot{\mathbf{u}}}(x), \quad \underline{\dot{\mathbf{u}}} \text{ periodic} \} \quad (10)$$

For the computation of the safety factor (or limit multiplier) s of the assigned macroscopic stress $\underline{\underline{\Sigma}}^o$, the kinematic formulation of limit analysis leads to the following constrained minimization problem:

$$s = \min_{\underline{\dot{\mathbf{u}}}, \underline{\dot{\mathbf{E}}}} \frac{1}{V} \int_V D(\underline{\dot{\mathbf{E}}}) dV \quad \text{subject to:} \quad (11)$$

$$\underline{\underline{\Sigma}}^o : \underline{\dot{\mathbf{E}}} = 1; \quad (12)$$

$$\underline{\dot{\mathbf{E}}} = \text{sym}(\text{grad} \underline{\dot{\mathbf{u}}}) + \underline{\dot{\mathbf{E}}} \text{ in } V; \quad \underline{\dot{\mathbf{u}}} \text{ periodic on } \Gamma \quad (13)$$

Two differences are worth noting between a customary structural kinematic limit analysis and problem (Eq. 11-13) encompassing homogenization and limit analysis combined: (i) the periodicity condition has to be satisfied by the term $\underline{\dot{\mathbf{u}}}$ of the velocity field on Γ ; (ii) the external actions applied to the RV are not accounted for through boundary conditions, but rather through an average condition expressed by Eq. 9 and normalization (Eq. 12).

4 Discrete formulation

Matrix notation will be adopted henceforth, e.g. bold-face symbols for matrices and vectors; macroscopic stresses and strain rates collected into vectors, namely:

$$\underline{\underline{\Sigma}}^T \equiv \{ \Sigma_{11} \quad \Sigma_{22} \quad \Sigma_{33} \quad \Sigma_{12} \quad \Sigma_{13} \quad \Sigma_{23} \};$$

$$\underline{\dot{\mathbf{E}}}^T \equiv \{ \dot{E}_{11} \quad \dot{E}_{22} \quad \dot{E}_{33} \quad 2\dot{E}_{12} \quad 2\dot{E}_{13} \quad 2\dot{E}_{23} \}.$$

Let all the material constituents (or phases) behave according to von Mises yield criterion defined by a single material parameter, i.e. the yield limit σ_0^p (p runs over the number of phases). When specialized to this criterion and rewritten in matrix notation, problem (Eq. 11-13) becomes:

$$s = \min_{\underline{\dot{\mathbf{u}}}, \underline{\dot{\mathbf{E}}}} \frac{1}{V} \sqrt{\frac{2}{3}} \sum_p \sigma_0^p \int_{V_p} \sqrt{\underline{\dot{\mathbf{E}}}^T \underline{\mathbf{X}} \underline{\dot{\mathbf{E}}}} dV \quad \text{subject to:} \quad (14)$$

$$\underline{\underline{\Sigma}}^T \underline{\dot{\mathbf{E}}} = 1; \quad \mathbf{Y}^T \underline{\dot{\mathbf{E}}} = 0 \text{ in } V; \quad (15)$$

$$\underline{\dot{\mathbf{E}}} = F(\underline{\dot{\mathbf{u}}}) + \underline{\dot{\mathbf{E}}} \text{ in } V; \quad \underline{\dot{\mathbf{u}}} \text{ periodic on } \Gamma \quad (16)$$

Eq. (15b) represents the incompressibility condition as a part of von Mises plasticity model. Eq. (16a) expresses geometric compatibility, F being the relevant linear differential operator. In Eq. 14-15 it has been set: $\mathbf{Y}^T \equiv \{ 1 \ 1 \ 1 \ 0 \ 0 \ 0 \}$ and $\mathbf{X} \equiv \text{diag}[\mathbf{I}, \frac{1}{2}\mathbf{I}]$, \mathbf{I} being the identity matrix of order 3.

Adopting now a conventional finite element discretization in space, in each element (marked by subscript e) the nodal velocities, gathered in vector $\underline{\dot{\mathbf{U}}}_e$, govern the modelled periodic velocity field $\underline{\dot{\mathbf{u}}}_e$ and the relevant strain rate field $\underline{\dot{\mathbf{E}}}_e$, respectively, through the relations:

$$\underline{\dot{\mathbf{u}}}_e = \mathbf{N}_e \underline{\dot{\mathbf{U}}}_e; \quad \underline{\dot{\mathbf{E}}}_e = \mathbf{B}_e \underline{\dot{\mathbf{U}}}_e; \quad (17)$$

where \mathbf{N}_e denotes the shape function matrix and \mathbf{B}_e the consequent compatibility matrix. Account taken of Eq. 3 and 17, the radicand in Eq. 14 reads:

$$\underline{\dot{\mathbf{E}}}^T \underline{\mathbf{X}} \underline{\dot{\mathbf{E}}} = \underline{\dot{\mathbf{E}}}^T \underline{\mathbf{X}} \underline{\dot{\mathbf{E}}} + 2\underline{\dot{\mathbf{E}}}^T \underline{\mathbf{X}} \mathbf{B}_e \underline{\dot{\mathbf{U}}}_e + \underline{\dot{\mathbf{U}}}_e^T \mathbf{R}_e \underline{\dot{\mathbf{U}}}_e, \quad (18)$$

where $\mathbf{R}_e \equiv \mathbf{B}_e^T \underline{\mathbf{X}} \mathbf{B}_e$.

Let all the element nodal velocity vectors $\underline{\dot{\mathbf{U}}}_e$ be assembled into the global periodic velocity vector $\underline{\dot{\mathbf{U}}}$ and, accordingly, the matrices \mathbf{B}_e , \mathbf{R}_e into the global matrices \mathbf{B} and \mathbf{R} , respectively.

If now the periodicity condition is enforced and rigid-body motions suppressed, a reduced vector $\underline{\dot{\mathbf{U}}}$ is generated from $\underline{\dot{\mathbf{U}}}$ and, consequently, reduced matrices \mathbf{B}^* and \mathbf{R}^* arise from \mathbf{B} and \mathbf{R} , respectively.

Account taken of the above provisions and adopting Gauss integration to numerically compute the integrals over the various phases (run by index p), the objective function (Eq. 14) is approximated as follows:

$$\sum_p \sigma_0^p \int_{V_p} \sqrt{\underline{\dot{\mathbf{E}}}^T \underline{\mathbf{X}} \underline{\dot{\mathbf{E}}}} dV \approx \sum_{r=1}^n \sigma_0^{p(r)} W_r |\mathbf{J}|_r \sqrt{\underline{\dot{\mathbf{E}}}^T \underline{\mathbf{X}} \underline{\dot{\mathbf{E}}} + 2\underline{\dot{\mathbf{E}}}^T \underline{\mathbf{X}} \mathbf{B}_r^* \underline{\dot{\mathbf{U}}}_r + \underline{\dot{\mathbf{U}}}_r^T \mathbf{R}_r^* \underline{\dot{\mathbf{U}}}_r} \quad (19)$$

where: index r runs over the set G of all n Gauss integration points ($r = 1 \dots n$) in the discretized RV ; W_r and $|\mathbf{J}|_r$ denote the integration weights and the determinant of the Jacobian matrix at Gauss point r , respectively.

Finally, expressing the incompressibility constraint (Eq. 15b) in terms of nodal periodic velocities and using Eq. 19, the finite element discrete formulation of problem (Eq. 14-16) becomes:

$$s \cong \min_{\underline{\dot{\mathbf{U}}}} \frac{1}{V} \sqrt{\frac{2}{3}} \sum_{r=1}^n \sigma_0^{p(r)} W_r |\mathbf{J}|_r \times \sqrt{\underline{\dot{\mathbf{E}}}^T \underline{\mathbf{X}} \underline{\dot{\mathbf{E}}} + 2\underline{\dot{\mathbf{E}}}^T \underline{\mathbf{X}} \mathbf{B}_r^* \underline{\dot{\mathbf{U}}}_r + \underline{\dot{\mathbf{U}}}_r^T \mathbf{R}_r^* \underline{\dot{\mathbf{U}}}_r} \quad (20)$$

subject to:

$$\underline{\underline{\Sigma}}^T \underline{\dot{\mathbf{E}}} = 1; \quad \mathbf{Y}^T (\mathbf{B}_r^* \underline{\dot{\mathbf{U}}}_r + \underline{\dot{\mathbf{E}}}) = 0 \quad r = 1 \dots n \quad (21)$$

The equality-constrained, convex mathematical programming problem (Eq. 20-21) exhibits two peculiar features: (a) the objective function is “nonsmooth”, in the sense that it is not differentiable for $\underline{\dot{\mathbf{E}}} = \mathbf{0}$; (b) the plastic incompressibility, Eq. 21b, required by von Mises plasticity model in combination with the finite element modelling of displacements, may give rise to “locking phenomena”, i.e. to excessive kinematic limitations on the set of possible (“admissible”) mechanisms, which might lead to an unrealistic increase of the resulting collapse multiplier s [Nagtegaal, Parks and Rice (1974)].

Various remedies for the latter difficulty (b) have been proposed and investigated in the literature. In particular, “mixed” finite element modelling was recently shown to eliminate or attenuate locking in limit analysis [Capsoni and Corradi (1997)]. As an alternative “antilocking” provision, already used e.g. in [Liu, Cen and Xu (1995)] and [Zhang, Zhang and Lu (1993)], a penalty procedure is adopted and implemented herein.

The former feature (a) would advocate recourse to concepts and formulations of “nonsmooth mathematics”, see e.g. [Mistakidis and Stavroulakis (1998)], for an appropriate modern theoretical framework. However, aiming at cost-effective numerical solutions to practical engineering purposes, use is made herein of the iterative algorithm which was proposed in [Huh and Yang (1991)], [Zhang, Zhang and Lu (1993)] and [Zhang and Lu (1995)] in order to circumvent the complication due to the circumstance (a).

The equality constraint (Eq. 21a) which expresses normalization of the “external power” will be dealt with by the customary Lagrange multiplier method.

As a consequence of the above chosen options, the augmented Lagrangian function associated to the (discrete, finite-dimensional) constrained minimization problem (Eq. 20-21) reads:

$$L(\tilde{\mathbf{U}}^*, \dot{\mathbf{E}}, \lambda) = \left\{ \frac{1}{V} \sqrt{\frac{2}{3}} \sum_{r=1}^n \sigma_0^{p(r)} W_r |\mathbf{J}|_r \times \sqrt{\dot{\mathbf{E}}^T \mathbf{X} \dot{\mathbf{E}} + 2 \dot{\mathbf{E}}^T \mathbf{X} \mathbf{B}_r^* \tilde{\mathbf{U}}^* + \tilde{\mathbf{U}}^{*T} \mathbf{R}_r^* \tilde{\mathbf{U}}^*} + \lambda (1 - \boldsymbol{\Sigma}^T \dot{\mathbf{E}}) + \frac{1}{2} \alpha \sum_{r=1}^n W_r |\mathbf{J}|_r \left(\dot{\mathbf{E}}^T \mathbf{C} \dot{\mathbf{E}} + 2 \dot{\mathbf{E}}^T \mathbf{C} \mathbf{B}_r^* \tilde{\mathbf{U}}^* + \tilde{\mathbf{U}}^{*T} \mathbf{Z}_r^* \tilde{\mathbf{U}}^* \right) \right\} \quad (22)$$

where: λ represents the unknown Lagrange multiplier; α the penalization factor (a datum to be suitably chosen); it has been set $\mathbf{C} \equiv \mathbf{Y} \mathbf{Y}^T$, $\mathbf{Z}_r^* \equiv \mathbf{B}_r^{*T} \mathbf{C} \mathbf{B}_r^*$.

The Kuhn-Tucker conditions for the stationarity of function L are expressed by the following set of nonlinear equations:

$$\frac{\partial L}{\partial \tilde{\mathbf{U}}^*} = \frac{1}{V} \sqrt{\frac{2}{3}} \sum_{r=1}^n \sigma_0^{p(r)} W_r |\mathbf{J}|_r \frac{\mathbf{R}_r^* \tilde{\mathbf{U}}^* + \mathbf{B}_r^{*T} \mathbf{X} \dot{\mathbf{E}}}{D_r} + \alpha \sum_{r=1}^n W_r |\mathbf{J}|_r \left(\mathbf{Z}_r^* \tilde{\mathbf{U}}^* + \mathbf{B}_r^{*T} \mathbf{C} \dot{\mathbf{E}} \right) = 0 \quad (23)$$

$$\frac{\partial L}{\partial \dot{\mathbf{E}}} = \frac{1}{V} \sqrt{\frac{2}{3}} \sum_{r=1}^n \sigma_0^{p(r)} W_r |\mathbf{J}|_r \frac{\mathbf{X} \mathbf{B}_r^* \tilde{\mathbf{U}}^* + \mathbf{X} \dot{\mathbf{E}}}{D_r} + \alpha \sum_{r=1}^n W_r |\mathbf{J}|_r \left(\mathbf{C} \mathbf{B}_r^* \tilde{\mathbf{U}}^* + \mathbf{C} \dot{\mathbf{E}} \right) - \lambda \boldsymbol{\Sigma} = 0 \quad (24)$$

$$\frac{\partial L}{\partial \lambda} = \boldsymbol{\Sigma}^T \dot{\mathbf{E}} - 1 = 0 \quad (25)$$

having set:

$$D_r \equiv \sqrt{\dot{\mathbf{E}}^T \mathbf{X} \dot{\mathbf{E}} + 2 \dot{\mathbf{E}}^T \mathbf{X} \mathbf{B}_r^* \tilde{\mathbf{U}}^* + \tilde{\mathbf{U}}^{*T} \mathbf{R}_r^* \tilde{\mathbf{U}}^*} \quad (26)$$

The above noted nonsmoothness of the objective function in Eq. 20 is reflected by the fact that the denominator D_r in Eqn. 23-24 vanishes whenever the r -th Gauss point does not exhibit plastic flow (i.e. “belongs to the rigid zone”). Provisions to tackle this circumstance are the main objective and the peculiar feature of the solution procedure that follows.

5 Iterative solution algorithm

To solve the system of nonlinear equations (Eq. 23-25), the algorithm devised first by Huh and Yang (1991) and further studied in [Zhang, Zhang and Lu (1993)], [Liu, Cen and Xu (1995)], [Zhang and Lu (1995)], implies the solution of the following set of linear equations:

$$\frac{1}{V} \sqrt{\frac{2}{3}} \sum_{r=1}^n \sigma_0^{p(r)} W_r |\mathbf{J}|_r \frac{\mathbf{R}_r^* \tilde{\mathbf{U}}^{*h} + \mathbf{B}_r^{*T} \mathbf{X} \dot{\mathbf{E}}^h}{H_r^{h-1}} + \alpha \sum_{r=1}^n W_r |\mathbf{J}|_r \left(\mathbf{Z}_r^* \tilde{\mathbf{U}}^{*h} + \mathbf{B}_r^{*T} \mathbf{C} \dot{\mathbf{E}}^h \right) = \mathbf{0} \quad (27)$$

$$\frac{1}{V} \sqrt{\frac{2}{3}} \sum_{r=1}^n \sigma_0^{p(r)} W_r |\mathbf{J}|_r \frac{\mathbf{X} \mathbf{B}_r^* \tilde{\mathbf{U}}^{*h} + \mathbf{X} \dot{\mathbf{E}}^h}{H_r^{h-1}} + \alpha \sum_{r=1}^n W_r |\mathbf{J}|_r \left(\mathbf{C} \mathbf{B}_r^* \tilde{\mathbf{U}}^{*h} + \mathbf{C} \dot{\mathbf{E}}^h \right) - \lambda^h \boldsymbol{\Sigma} = \mathbf{0} \quad (28)$$

$$\boldsymbol{\Sigma}^T \dot{\mathbf{E}}^h = 1 \quad (29)$$

where $\tilde{\mathbf{U}}^{*h}$, $\dot{\mathbf{E}}^h$ and λ^h are the unknowns at the current, say h , iteration. On the basis of the results obtained at iteration $h-1$, let the set of Gauss integration points G be subdivided into a subset P^{h-1} (“plastic zone”) of the points where dissipation occurs, and the complementary subset R^{h-1} (“rigid zone”) of the points where the computed plastic strain rates are such that the denominator D_r^{h-1} , in Eq. 23-24, is below a suitably chosen tolerance $\beta \ll 1$. Following Zhang, Zhang and Lu (1993), another available parameter $\gamma \ll 1$ is selected and the denominator in Eq. 27-28 is defined as:

$$H_r^{h-1} = \begin{cases} D_r^{h-1} & \forall r \in P^{h-1} \\ \gamma \ll 1 & \forall r \in R^{h-1} \end{cases} \quad (30)$$

By virtue of this provision, the iterative procedure can proceed smoothly. Since H_r^{h-1} is now a datum derived from the preceding iteration $h-1$, linear Eq. 27-29 can be cast in the following compact form:

$$\mathbf{A}^{h-1} \tilde{\mathbf{U}}^{*h} + \mathbf{M}^{h-1T} \dot{\mathbf{E}}^h = \mathbf{0} \quad (31)$$

$$\mathbf{M}^{h-1} \tilde{\mathbf{U}}^{*h} + \mathbf{N}^{h-1} \dot{\mathbf{E}}^h = \lambda^h \boldsymbol{\Sigma} \quad (32)$$

$$\boldsymbol{\Sigma}^T \dot{\mathbf{E}}^h = 1 \quad (33)$$

The new symbols for the coefficient matrices in Eq. 31-33 have the following meanings:

$$\mathbf{A}^{h-1} \equiv \frac{1}{V} \sqrt{\frac{2}{3}} \sum_{r=1}^n \sigma_0^{p(r)} W_r |\mathbf{J}|_r \frac{\mathbf{R}_r^*}{H_r^{h-1}} + \alpha \sum_{r=1}^n W_r |\mathbf{J}|_r \mathbf{Z}_r^* \quad (34)$$

$$\mathbf{M}^{h-1} \equiv \frac{1}{V} \sqrt{\frac{2}{3}} \sum_{r=1}^n \sigma_0^{p(r)} W_r |\mathbf{J}|_r \frac{\mathbf{X} \mathbf{B}_r^*}{H_r^{h-1}} + \alpha \sum_{r=1}^n W_r |\mathbf{J}|_r \mathbf{C} \mathbf{B}_r^* \quad (35)$$

$$\mathbf{N}^{h-1} \equiv \frac{1}{V} \sqrt{\frac{2}{3}} \sum_{r=1}^n \sigma_0^{p(r)} W_r |\mathbf{J}|_r \frac{\mathbf{X}}{H_r^{h-1}} + \alpha \sum_{r=1}^n W_r |\mathbf{J}|_r \mathbf{C} \quad (36)$$

Let vectors \mathbf{V}^{*h} and \mathbf{S}^h denote the solution of the linear system consisting of Eq. 31 and 32 alone, with $\lambda^h = 1$. Then the solution of the whole system (Eq. 31- 33) is readily seen to be:

$$\hat{\mathbf{U}}^{*h} = \lambda^h \mathbf{V}^{*h}; \quad \hat{\mathbf{E}}^h = \lambda^h \mathbf{S}^h; \quad \lambda^h = \frac{1}{\boldsymbol{\Sigma}^T \mathbf{S}^h} \quad (37)$$

As a convenient initialization (at iteration $h = 1$) of the iterative procedure centred on Eq. 27-29, the *RV* is assumed to be in a fully plastic state by setting $D_r^0 = 1$, $r = 1 \dots n$.

At the end of each (h -th) iteration, a value s^h of the limit multiplier of the assigned macroscopic stresses $\boldsymbol{\Sigma}$ is computed as:

$$s^h = \frac{1}{V} \sqrt{\frac{2}{3}} \sum_{r=1}^n \sigma_0^{p(r)} W_r |\mathbf{J}|_r D_r^h \quad (38)$$

The iteration sequence is stopped when either one of the following convergence criteria is satisfied:

$$\frac{|\mu^{h-1} - \mu^h|}{\mu^{h-1}} \leq \delta_1, \quad \frac{\|\hat{\mathbf{U}}^{h-1} - \hat{\mathbf{U}}^h\|}{\|\hat{\mathbf{U}}^{h-1}\|} \leq \delta_2 \quad (39)$$

where δ_1, δ_2 are suitably chosen tolerances and $\|\dots\|$ denotes Euclidean norm.

The penalty factor α (see Eq. 27-28), introduced to enforce “softly” the constitutive requirement of plastic incompressibility, can either be suitably modified or take a fixed value during the iterative process. To the authors’ knowledge, general criteria for initializing and updating penalty factors do not exist, despite a fairly extensive literature on penalty methods, see e.g. [Fiacco and McCormick (1968)]. Some criteria have been proposed (e.g. in [Bertsekas (1982)]) for particular classes of problems and often they do not give satisfactory results when applied to other contexts. The numerical simulations carried out herein show that keeping the value of the penalty factor fixed during the iterative procedure does not lead to results worse than the ones obtained by updating the factor at each iteration. Therefore, in the present implementations and applications of the kinematic approach the penalty factors do not change during the iterative solution.

Numerical experiences, such those to be discussed in the next Section, show that the above outlined iterative process, with a suitable problem-dependent empirically based choice of the available parameters, leads to a satisfactory approximation of the limit load multiplier s and to a collapse mechanism $\hat{\mathbf{U}}$ through a fast convergent sequence of iterations with monotonically decreasing s^h .

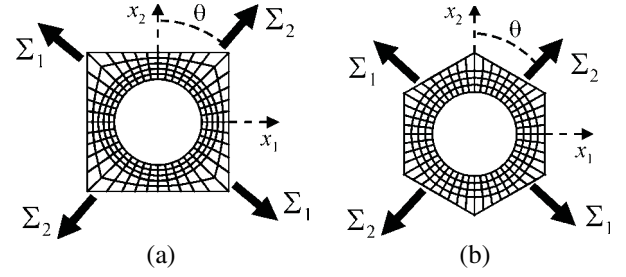


Figure 1 : (a) square, (b) hexagonal *RV* of perforated periodic plates.

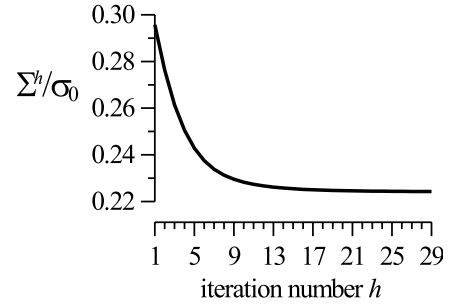


Figure 2 : Convergence of the macroscopic stress Σ_2 ($\Sigma_1 = 0$, $\theta = 0^\circ$) to the limit value for a square *RV* with $c_h = 0.5$

6 Comparative tests and applications

6.1 Perforated plates

Evenly perforated metal plates, with holes arranged according to either square or hexagonal patterns, are employed in several engineering systems (e.g. as tubesheet heat exchangers in power plants). The potentialities of the direct kinematic method to predict the macroscopic strength properties of this class of period media are assessed below, by analyzing the unit cells depicted in Fig. 1a and Fig. 1b, which describe, respectively, square and hexagonal perforation patterns.

Numerical investigations are carried out for biaxial states of macroscopic stresses, with a given ratio of the two nonvanishing principal stresses Σ_1 and Σ_2 (Fig. 1a,b), at different angles between the principal stress directions and the symmetry axes of the cells.

The numerical investigations on the square *RV* with circular hole are performed assuming a mesh of 200 four-noded isoparametric finite elements and 240 nodes with two d.o.f.s each (Fig. 1a). The hexagonal *RV* with circular hole is discretized by 192 four-noded isoparametric finite elements and 240 nodes with two d.o.f.s each (Fig. 1b).

In the present analyses of both the square and the hexagonal cell with circular hole, the desired numerical accuracy is satisfied setting δ_1 and δ_2 in Eq. 39 equal to 10^{-4} .

The plate is interpreted as a plane-stress structure. Therefore

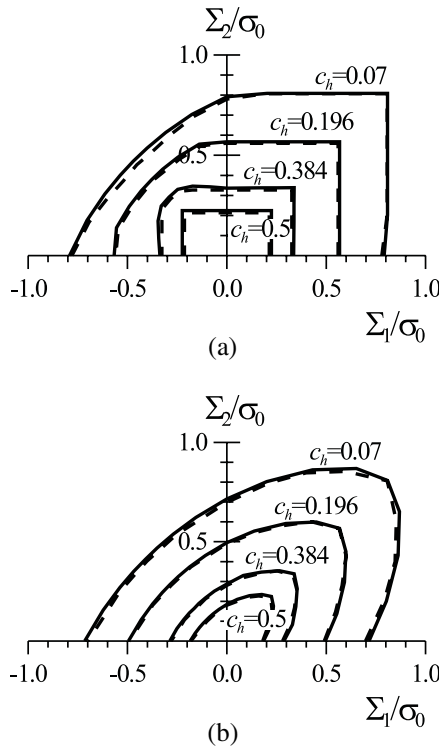


Figure 3 : Square RV with circular hole. Limit macroscopic stress domains for different hole volume fractions c_h . Comparison between the present method (solid line) and Rogalska, Kakol, Guerlement and Lamblin (1997) (dashed line). (a) $\theta = 0^\circ$, (b) $\theta = 45^\circ$.

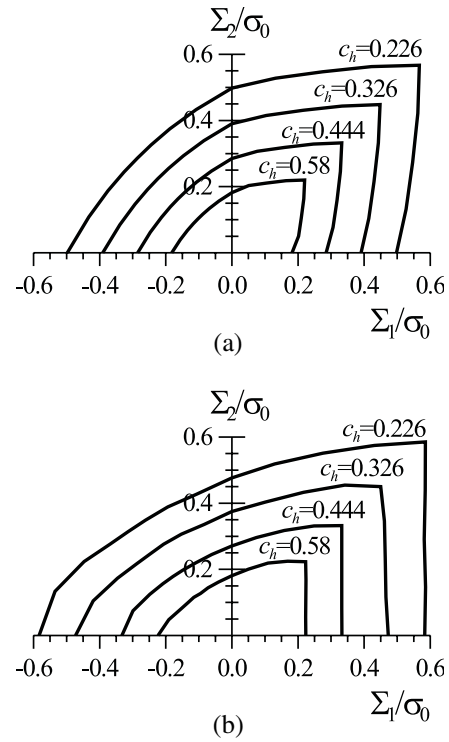


Figure 4 : Hexagonal RV with circular hole. Limit yield domains in macroscopic stresses for different hole volume fractions c_h . (a) $\theta = 15^\circ$, (b) $\theta = 30^\circ$.

plastic incompressibility needs not be enforced explicitly and, hence, the quantity γ ($\gamma = \beta$), see Eq. 30, is the only available parameter involved in the present limit analysis problem: it is set here equal to 10^{-10} .

For illustration, the monotonic convergence of the macroscopic stress Σ to the limit value is depicted in Fig. 2 for a square RV with hole volume fraction $c_h = 0.5$, subjected to uniaxial tension along x_2 .

The (macroscopic) strength of the homogenized medium equivalent to the perforated plate under biaxial plane stress conditions is to be determined for a given orientation θ of principal average stress Σ_2 with respect to axis x_2 . The strength domain can be defined approximately point by point, by following radial paths in the plane (Σ_1, Σ_2) and computing the limit load multiplier s according to the kinematic definition of the macroscopic strength domain S^{hom} (see Eq. 10).

Consider first a square perforation pattern. The present method is tested by comparisons with the results achieved by a method proposed in [Rogalska, Kakol, Guerlement and Lamblin (1997)] which is not based on the homogenization theory for periodic media. In [Rogalska, Kakol, Guerlement and Lamblin (1997)] the prediction of the macroscopic yield do-

main for a thin specimen with a square pattern of circular holes was carried out by means of a commercial finite element code and incremental (step-by-step) analyses. This approach is able to predict only the yield domains for two orientations: $\theta = 0^\circ$ and $\theta = 45^\circ$ by imposing customary (not periodicity) boundary conditions in view of the symmetries for the above two particular orientations. Despite the difference in theoretical origins, the two methods supply macroscopic strength domains that are in good agreement over a wide range of hole volume fractions for both the considered orientations θ (see Fig. 3a,b).

Consider now a disk with a hexagonal perforation pattern of circular holes, i.e. a case not investigated in the literature, to the authors' knowledge.

In Fig. 4 the macroscopic strength domains of plates with hole volume fraction varying from 0.226 to 0.58 have been determined for $\theta = 15^\circ$ (Fig. 4a) and $\theta = 30^\circ$ (Fig. 4b). The potentialities of the proposed numerical method based on the homogenization theory for periodic media and on the kinematic approach to limit analysis are highlighted whenever symmetry simplifications are not allowed for the kinematic boundary conditions on the RV.

6.2 Fiber-reinforced composites

In view of their peculiar mechanical properties, unidirectional fiber-reinforced composites (FRCs), especially metal-matrix composites (MMC), are widely used by space and aeronautical industries [see e.g. Dvorak, Lagoudas, and Huang (1994)]. They are particularly suited to technological situations where high stiffness, strength and ductility are required. Their importance in the above mentioned and other fields confers practical interest to the cost-effective evaluation of the strength domain for unidirectional fiber-reinforced composites. “Phenomenological” semiempirical strength criteria for FRCs, such as those proposed in [Tsai and Wu (1971)], can often be conveniently employed to analyze structural members made of composites. However, when the macroscopic properties of FRCs must be predicted on the basis of the local properties of the components, a micromechanical approach is needed.

The usage of homogenization for periodic media in the framework of limit analysis has led to theoretical bounds on the macroscopic strength domain of unidirectional FRCs in semi-analytical form (see e.g. [Taliervo (1992)]).

In many cases these bounds are not sufficiently close to each other and, therefore, numerical methods have to be employed to achieve reliable estimates of the material macroscopic strength. In this context the proposed kinematic method is intended to predict the macroscopic yield domain S^{hom} of the homogeneous material “equivalent” to the periodic composites considered herein.

The assumption that the fibers are distributed according to a regular pattern reduces the prediction of macroscopic properties to the analysis of the *RV*, which is considerably easier than taking into account randomness in the reinforcing array. Square and hexagonal arrangements of fibers are often considered. A hexagonal pattern (Fig. 5a) was shown in [Brockenbrough, Suresh and Wienecke (1991)] to be especially suitable to predict the macroscopic properties of FRCs and, hence, will be employed herein to assess the potentialities of the proposed numerical method in computing the uniaxial strength of the homogenized material. A square cell (Fig. 5b) will also be adopted in some applications, mostly for comparisons with the results of other authors. Metal-matrix two-phase composites are considered, with both phases complying with von Mises plasticity model σ_0^f and σ_0^m denoting the yield stresses of the fibers and of the matrix, respectively.

6.2.1 Transverse tensile tests

Consider first uniaxial states of macroscopic stresses in the plane x_1 - x_2 perpendicular to the fiber direction. Let θ denote the angle between the macroscopic tension Σ and the symmetry axis x_2 of the *RV* (see Fig. 5). As pointed out in [Michel and Suquet (1993)], in this case computations should be performed under “generalized” plane-strain hypothesis, which is therefore adopted here, in order to assess its accuracy by com-

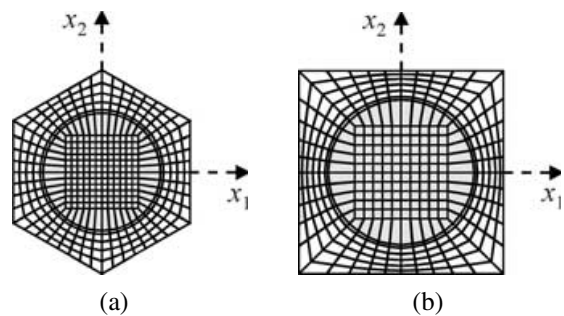


Figure 5 : (a) hexagonal and (b) square *RV* with circular fiber.

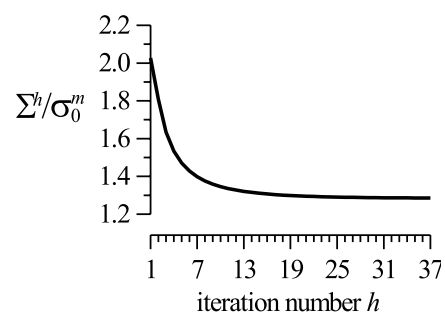


Figure 6 : Hexagonal *RV* with circular fiber: $c_f = 0.5$, $\sigma_0^f/\sigma_0^m = 5$, $\theta = 0^\circ$. Convergence of the macroscopic stress to its limit value, for $\alpha = 10^6$ and $\gamma = 10^{-10}$.

parison with available results.

The hexagonal cell of Fig. 5a is subdivided into 432 four-node isoparametric elements with 457 nodes.

In the generalized plane-strain formulation the present direct iterative method requires to apriori choose the values of the parameters α and γ ($\gamma = \beta$), see Sec. 4: the factor γ concerning the rigid zone is assumed to be 10^{-10} , the penalty factor enforcing the incompressibility condition is set equal to 10^6 . The tolerance parameters δ_1, δ_2 are chosen equal to 10^{-4} . The constitutive ratio σ_0^f/σ_0^m is taken equal to 5. For a FRC with fiber volume fraction $c_f = 0.5$, the convergence of the iterative procedure in terms of macroscopic limit stress acting along x_2 axis is visualized in Fig. 6.

The macroscopic transverse tensile strength predicted by the present kinematic method is plotted in Fig. 7 versus the orientation θ , for a cell with c_f equal to 0.25 and 0.5. The results obtained by the evolutive method proposed in [Michel and Suquet (1993)] are also drawn for comparison.

The two finite element analyses predict the same trend of the limit macroscopic stress with the orientation angle θ . The present approach leads to slightly higher values than the other numerical one. The maximum difference between the results compared is less than 2% and occurs at $\theta = 15^\circ$.

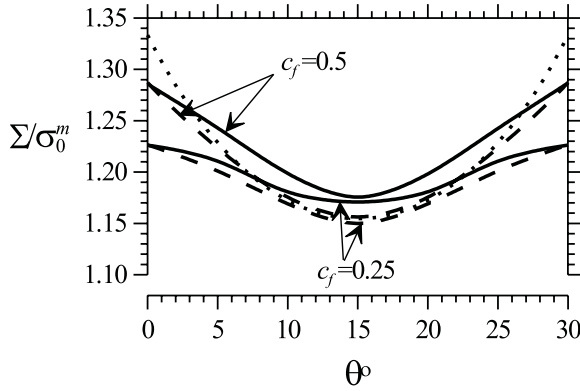


Figure 7 : Hexagonal RV with circular fiber and with $\sigma_0^f/\sigma_0^m = 5$. Limit macroscopic stress vs angle θ . Comparison between the present method (solid line), Michel and Suquet (1993) (dashed line) and Taliercio’s (1992) upper bound (dotted line).

It is interesting to compare the present numerical results to the bounds provided by the method presented in [Taliercio (1992)], based on the application of the kinematic theorem of limit analysis to homogenization theory for periodic media. According to that method, an upper bound on the “support function” [Tyrrel Rockafellar (1970)] of the macroscopic strength domain of the composite, π^{hom} is given by:

$$\pi^{hom}(\underline{\dot{E}}) \leq \frac{1}{V} \left(\int_V \pi(\underline{\dot{\varepsilon}}) dV + \int_S \pi(\underline{n}; [[\underline{\dot{u}}]]) dS \right) \quad (40)$$

where the right-hand side can be mechanically interpreted as the power dissipated in any failure mechanism for the cell conforming to the periodicity of the medium, with $\underline{\dot{u}}$, $\underline{\dot{\varepsilon}}$ and $\underline{\dot{E}}$ fulfilling Eq. 3 and 5. The second term is the power dissipated along discontinuity surface S for the microscopic velocity field power, \underline{n} being locally the unit normal to S and $[[\underline{\dot{u}}]]$ the jump in velocity across S (see [Taliercio (1992)] for further details).

In the case of MMCs with periodic hexagonal reinforcing array and matrix complying with the von Mises criterion, if mechanisms characterized by slip planes with $\underline{n} = \frac{e_1}{6} \cos(\frac{\pi}{6}(1+2m)) + \frac{e_2}{6} \sin(\frac{\pi}{6}(1+2m))$ ($m = 0, 1, \dots$), are considered (see the case $m = 1$ in Fig. 8a), the upper bound on the support function of S^{hom} specializes to:

$$\pi^{hom}(\underline{\dot{E}}) \leq \frac{l\sigma_0^m}{V} \nu \quad (41)$$

where

$$\underline{\dot{E}} = \frac{\sqrt{3}l}{4V} (\sqrt{3}(\underline{e}_2 \otimes \underline{e}_2 - \underline{e}_1 \otimes \underline{e}_1) + \underline{e}_1 \otimes \underline{e}_2 + \underline{e}_2 \otimes \underline{e}_1) \nu \quad (42)$$

if $m = 0$;

$$\underline{\dot{E}} = \frac{\sqrt{3}l}{2V} (\underline{e}_1 \otimes \underline{e}_2 + \underline{e}_2 \otimes \underline{e}_1) \nu \quad \text{if } m = 1; \text{ etc.} \quad (43)$$

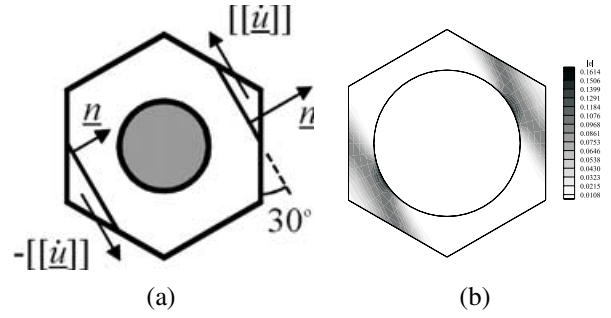


Figure 8 : (a) Collapse mechanism for Taliercio’s (1992) upper bound; (b) contour plot of the equivalent strain rate field at collapse for $c_f = 0.5$, $\sigma_0^f/\sigma_0^m = 5$, $\theta = 15^\circ$ by the present method.

In Eq. 41-43, ν denotes the modulus of the velocity jump $[[\underline{\dot{u}}]]$ (which is assumed to be parallel to the slip plane and orthogonal to x_3) and l is the length of each side of the RV cell.

When applied to the prediction of upper bounds on the transverse tensile strength of the composite along any direction $\underline{e}_\theta = \underline{e}_1 \cos \theta + \underline{e}_2 \sin \theta$, so that $\underline{\underline{\Sigma}} = \Sigma \underline{e}_\theta \otimes \underline{e}_\theta$, the above results give:

$$\Sigma \leq \min \left\{ \frac{2\sigma_0^m}{\sqrt{3} \sin 2\theta}; \frac{4\sigma_0^m}{\sqrt{3} (\sqrt{3} \cos 2\theta + \sin 2\theta)} \right\} \quad (44)$$

with $0 \leq \theta \leq 60^\circ$ according to the hexagonal periodicity of the heterogeneous medium considered.

This theoretical bound is plotted in Fig. 7 together with the present and other numerical predictions. A good agreement is observed. In the case of the proposed numerical model, this agreement can be explained by considering the failure mechanisms associated to the collapse load factor computed for any θ : the case $\theta = 15^\circ$ is illustrated in Fig. 8b, where the equivalent strain rate distribution at collapse is represented. The simple failure mechanism considered (Fig. 8a), estimating upper bounds to the macroscopic transverse strength of the composite, qualitatively matches the “exact” mechanism detected by more sophisticated numerical models.

The results of both finite element methods are slightly exceeded by the analytical upper bound for $\theta \cong 0$ and $\theta \cong 30^\circ$. It is worth noting that this agreement comes from the choice made here for the fiber volume fraction: with higher percentages of reinforcement, the theoretical upper bounds are no longer meaningful [Taliercio (1992)] and resort to numerical methods is practically compulsory.

6.2.2 Off-axis tensile tests

In order to predict the macroscopic off-axis tensile strength of a FRC, the analysis of the representative volume must take into account its three-dimensional deformation modes. By virtue of

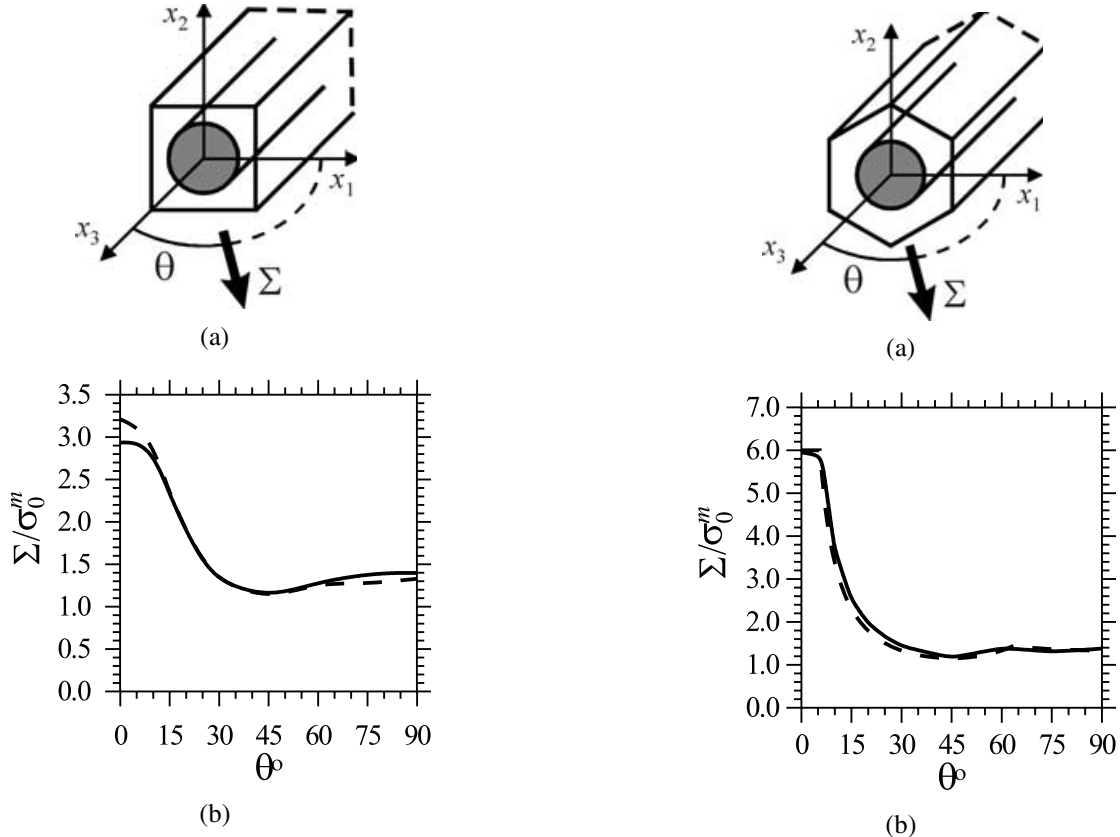


Figure 9 : (a) MMC with square reinforcing array, $c_f = 0.49$, $\sigma_0^f/\sigma_0^m = 5$; (b) macroscopic off-axis strength vs angle θ predicted by the present method (solid line) and Francescato and Pastor (1997) (dashed line).

the assumed unlimited length of the fibers, all cross-sections of the RV exhibit equal deformed shape, that is representative of such deformation modes: this means that the microscopic strain rate field over the RV has to be such that (see also [Francescato and Pastor (1997)]):

$$\tilde{\epsilon}_{ij} = \tilde{\epsilon}_{ij}(x_1, x_2) \quad \forall ij \neq 33; \quad \tilde{\epsilon}_{33} = 0 \quad (45)$$

By considering 3D velocity fields (Eq. 5) complying with the above condition, numerical analyses were carried out on the discretized cells shown in Fig. 5a and Fig. 5b subjected to uniaxial tension in the plane (x_1, x_3) . The penalty factor α , the factor γ and the tolerance parameters δ_1 , δ_2 have been given the same values as in the preceding generalized plane strain analysis (Sec. 6.2.1).

Two different MMCs were considered, for which numerical and analytical results by other authors were available. The first one is a composite analyzed in [Francescato and Pastor (1997)], reinforced by fibers arranged according to a square pattern with $c_f = 0.49$, $\sigma_0^f/\sigma_0^m = 5$ (see Fig. 9a). The second one is a MMC with hexagonal reinforcing array, $c_f = 0.65$, $\sigma_0^f/\sigma_0^m = 8.7$, (see Fig. 10a), the limit strength of which was

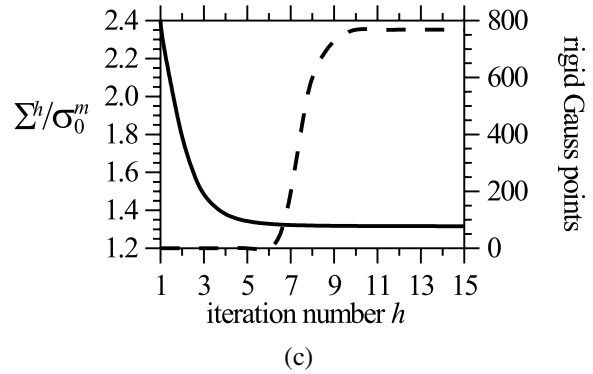


Figure 10 : (a) Hexagonal RV with circular fiber: $c_f = 0.65$, $\sigma_0^f/\sigma_0^m = 8.7$; (b) macroscopic off-axis strength vs angle θ predicted by the present method (solid line) and Taliencio (1992) (dashed line); (c) convergence of the macroscopic stress to its limit value (solid line) and evolution of the rigid zones (dashed line) for $\alpha = 10^6$ and $\gamma = 10^{-10}$.

analytically predicted in [Taliencio (1992)].

In Fig. 9b, the macroscopic off-axis tensile strength provided by the present approach for the first MMC is plotted versus the orientation θ of the applied stress Σ to the fiber axis x_3 . The obtained results are compared to those obtained in [Francescato and Pastor (1997)] by means of an algorithm based on the piecewise linearization of the yield surface and

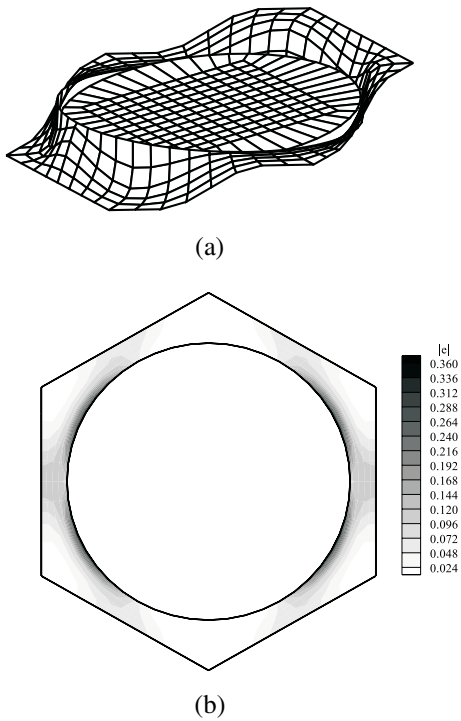


Figure 11 : Hexagonal RV with circular fiber, $c_f = 0.65$, $\sigma_0^f/\sigma_0^m = 8.7$, $\theta = 75^\circ$: (a) deformed mesh and (b) contour plot of the equivalent plastic strain rate corresponding to the computed collapse multiplier.

linear programming (LP). The agreement between the results is quite satisfactory. The computational cost inherent in the LP method, on the basis of our experiences with LP approaches, can be reasonably conjectured to be significantly reduced with the present one.

The results of the analyses carried out on the second MMC are summarized in Fig. 10. In Fig. 10b the off-axis strengths predicted by the present procedure and by the analytical model in [Talierecio (1992)] based on homogenization and limit analysis are plotted versus the orientation of the applied stress to the fibers.

As shown in [Talierecio (1992)], an upper bound on the macroscopic uniaxial strength of the composite, computed according to the same path of reasoning outlined in the preceding paragraph, is given by

$$\Sigma \leq \min \left\{ \sigma_0^m \left[1 + c_f \left(\frac{\sigma_0^f}{\sigma_0^m} - 1 \right) \right]; \frac{2\sigma_0^m}{\sqrt{3} \sin 2\theta}; \frac{2\sigma_0^m}{\sin \theta \sqrt{3(1 - \sin^2 \theta/4)}} \right\} \quad (46)$$

These bounds were computed using failure mechanisms for

the cell characterized by uniform strain rate (first bound), or by slip planes of the type already shown in Fig. 8a, but with an out-of-plane component of the relative velocity between the rigid blocks (second and third bound). The agreement between numerical and analytical results is excellent and suggests the possibility of obtaining reliable results by the present approach also in those situations where the analytical methods is bound to fail (namely, if c_f is high and prevents the development of slip planes cutting only the matrix).

Fig. 10c shows that the collapse multiplier rapidly converges to its final value, and reaches an asymptote when the plastic zones localize, as shown by the sudden increase in the number of “rigid” Gauss points, apparent in the same figure.

The numerically computed “failure mechanism” is shown in Fig. 11 for the orientations $\theta = 75^\circ$ of the uniaxial macroscopic stress Σ to the fibers. This figure shows both the deformed mesh (Fig. 11a) and the contour plots of the equivalent plastic strain rate (Fig. 11b) corresponding to the computed collapse multiplier. The fiber is apparently not involved in the mechanism, according to its high yield stress, and the plastic zones are localized around shear bands that agree with the slip planes considered in [Talierecio (1992)] in order to compute an analytical upper bound on the macroscopic yield stress.

7 Conclusions

A finite element numerical procedure has been developed and numerically tested apt to predict, by a direct (nonevolutive) kinematic approach, the strength (i.e. the average stresses carrying capacity) and the limit behavior at plastic collapse, of perfectly-plastic periodic heterogeneous media, such as perforated plates and metal-matrix composites. Essential features of the procedure investigated herein are as follows.

1. The yield domain is sought in the space of the macroscopic (average) stresses, on the basis of the kinematic theorem of classical limit analysis for von Mises material models.
2. Reference is made to a single unit cell as “representative volume”, in the framework of homogenization theory, i.e. by imposing periodicity on its boundary and confining to it the finite element discretization.
3. The plastic incompressibility requirement is softly enforced by suitable penalization, thus avoiding “locking” manifestations.
4. The numerical solution algorithm transforms the non-linear, non-smooth mathematical optimization problem leading to the “safety factor” into a sequence of linear problems. Convergence of the iterative algorithm has been numerically investigated as for the choice of available parameters (in primis of the penalty factor), and favorably assessed with reference to specific cases.

5. The accuracy of the present kinematic limit analysis technique has been verified through comparisons with results available in the literature concerning the analysis of periodically heterogeneous elastoplastic media up to failure. The “direct” method in point turns out to be definitely superior in terms of computational cost with respect to evolutive analyses. It is not subjected to the restrictions inherent to existing semi-analytical methods [Taliervo (1992)], since it is applicable to media with any heterogeneity volume fraction.
6. In particular, as for the crucial choice of the penalty factor for the enforcement of the incompressibility condition, in the absence of “*a priori*” criteria for a given set of problem data, a fairly wide range of values leading to convergence on the actual safety factor s have been determined by means of numerical experiences. The results were confirmed by comparisons with those achieved by other methods. The ranges of suitable penalty factors found herein can reasonably be employed in applications to heterogeneous media basically similar to the ones considered here (but a diverse type of applications might call for a different choice of these values).

Work in progress concerns the extension of the present method to the shakedown analysis of ductile composites subjected to variable-repeated thermomechanical loads, in order to compute domains of adaptation of the unit cell in the space of the macroscopic stresses [Carvelli, Maier and Taliervo (1999)]. Future extensions of this study will concern the prediction of the macroscopic strength of periodically reinforced materials with weakening interfaces, which are a possible source of non-associativity in the homogenized behavior.

Acknowledgement: A research grant from CNR (Italian Research Council) within the national coordinated project on “Materials for advanced technologies” (contract n. 97.00906.PF34) is gratefully acknowledged.

References

- Aboudi, J.** (1991): *Mechanics of composite materials*. Elsevier.
- Bertsekas, D. P.** (1982): *Constrained optimization and Lagrange multiplier methods*. Academic Press Inc.
- Bouchitte, G.; Suquet, P.** (1991): Homogenization, plasticity and yield design. In Dal Maso, G.; Dell’Antonio, G. F.(Eds): *Composite media and homogenization theory*. Birkhauser, Boston.
- Brockenbrough, J. R.; Suresh, S.; Wienecke, H. A.** (1991): Deformation of metal-matrix composites with continuous fibers: geometrical effects of fiber distribution and shape. *Acta Metall. Mater.*, vol. 39, pp. 735–752.
- Capsoni, A.; Corradi, L.** (1997): A finite element formulation of the rigid-plastic limit analysis problem. *Int. J. Num. Meth. Eng.*, vol. 40, pp. 2063–2086.
- Carvelli, V.; Maier, G.; Taliervo, A.** (1998): Limit analysis of periodic composites by a kinematic approach. In Crivelli Visconti, I.(Ed): *ECCM-8 European Conference on Composite Materials*. Naples, Woodhead Publishing Limited, vol. 4, pp. 389–396.
- Carvelli, V.; Maier, G.; Taliervo, A.** (1999): Shakedown analysis of periodic heterogeneous materials by a kinematic approach. *Mechanical Engineering (Strojnický Časopis)*, vol. 50, no. 4, pp. 229–240.
- Cohn, M. Z.; Maier, G.** (1979): *Engineering plasticity by mathematical programming*. Pergamon Press, New York.
- de Buhan, P.; Maghous, S.** (1991): Une méthode numérique pour la détermination du critère de résistance macroscopique de matériaux hétérogènes à structure périodique. *C. R. Acad. Sci. Paris*, t. 313, Série II, pp. 983–988.
- Dvorak, G. J.; Lagoudas, D.; Huang, C. M.** (1994): Fatigue damage and shakedown in metal matrix composite laminates. *Mech. Composite Mat. Struct.*, vol. 1, pp. 171–202.
- Fiacco, A. V.; McCormick, G. P.** (1968): *Nonlinear Programming: Sequential Unconstrained Minimization Techniques*. John Wiley & Sons, New York.
- Francescato, P.; Pastor, J.** (1997): Lower and upper numerical bounds to the off-axis strength of unidirectional fiber-reinforced composites by limit analysis methods. *Eur. J. Mech. /A Solids*, vol. 16, pp. 213–234.
- Hashin, Z.** (1983): Analysis of composite materials - a survey. *J. Appl. Mech.*, vol. 50, pp. 481–505.
- Huh, H.; Yang, W. H.** (1991): A general algorithm for limit solutions of plane stress problems. *Int. J. Sol. Struct.*, vol. 28, pp. 727–738.
- Liu, Y. H.; Cen, Z. Z.; Xu, B. Y.** (1995): A numerical method for plastic limit analysis of 3-d structures. *Int. J. Sol. Struct.*, vol. 32, pp. 1645–1658.
- Lubliner, J.** (1990): *Plasticity theory*. Macmillan Publishing Company.
- Maier, G.; Drucker, D. C.** (1973): Effects of geometry change on essential features of inelastic behaviour. In *Proceedings ASCE, Journal of the Engineering Mechanics Division 99 N.EM4*, pp. 819–834.
- Michel, J.; Suquet, P.** (1993): On the strength of composites materials: variational bounds and computational aspects. In Bendsøe, M. P.; Mota-Soares, C. A.(Eds): *Topology Design of Structures*, pp. 355–374. Kluwer Publishers.

Mistakidis, E. S.; Stavroulakis, G. E. (1998): *Nonconvex optimization in mechanics*. Kluwer Academic Publishers.

Nagtegaal, J. C.; Parks, D. M.; Rice, J. R. (1974): On numerically accurate finite element solutions in the fully-plastic range. *Comp. Meth. Appl. Mech. Eng.*, vol. 4, pp. 153–177.

Nemat-Nasser, S.; Hori, M. (1993): *Micromechanics: overall properties of heterogeneous materials*. North-Holland series in Applied Mathematics and Mechanics.

Rogalska, E.; Kakol, W.; Guerlement, G.; Lamblin, D. (1997): Limit load analysis of perforated disks with square penetration pattern. *J. Press. Vessel Technology*, vol. 119, pp. 122–126.

Suquet, P. (1983): Analyse limite et homogénéisation. *C. R. Acad. Sci. Paris*, t. 296, Série II, pp. 1355–1357.

Suquet, P. (1985): Elements of homogenization for inelastic solid mechanics. In *CISM Lectures, Homogenization techniques for composite media*. Springer-Verlag.

Taliervo, A. (1992): Lower and upper bounds to the macroscopic strength domain of a fiber-reinforced composite material. *Int. J. of Plasticity*, vol. 8, pp. 741–762.

Taliervo, A.; Sagramoso, P. (1995): Uniaxial strength of polymeric-matrix fibrous composites predicted through a homogenization approach. *Int. J. Sol. Struct.*, vol. 32, pp. 2095–2123.

Teply, J. L.; Dvorak, G. J. (1988): Bounds on overall instantaneous properties of elastic-plastic composites. *J. Mech. Phys. Solids*, vol. 36, pp. 29–58.

Tsai, S. W.; Wu, E. M. (1971): A general theory of strength for anisotropic materials. *J. Comp. Mater.*, vol. 5, pp. 58–80.

Tyrrel Rockafellar, R. (1970): *Convex analysis*. Princeton University Press, Princeton.

Zhang, Y. G.; Lu, M. W. (1995): An algorithm for plastic limit analysis. *Comp. Meth. Appl. Mech. Eng.*, vol. 126, pp. 333–341.

Zhang, Y. G.; Zhang, P.; Lu, M. W. (1993): Computational limit analysis of rigid-plastic bodies in plane strain. *Acta Mech. Sol. Sinica*, vol. 6, pp. 341–348.